Automation in Construction 109 (2020) 102986

Contents lists available at ScienceDirect

Automation in Construction

journal homepage: www.elsevier.com/locate/autcon

Direct printing test for buildability of 3D-printable concrete considering economic viability

Venkatesh Naidu Nerella[a,*], Martin Krause[b], Viktor Mechtcherine[a]

[a] Institute of Construction Materials, Technische Universität Dresden, Von-Mieses-Bau, 3 O.G., Georg-Schumann-Str. 07, 01087 Dresden, Germany
[b] Institute of Construction Management, Technische Universität Dresden, Nürnberger Straße 31A, 01187 Dresden, Germany

A B S T R A C T

Buildability, i.e. the ability of a deposited material bulk to retain its dimensions under increasing load, is an inherent prerequisite for formwork-free digital concrete construction (DC). Since DC processes are relatively new, no standard methods of characterization are available yet. The paper presents direct printing test as a practice-oriented approach, in which buildability test parameters are determined by taking various process aspects and construction costs into consideration. In doing so, direct links between laboratory buildability tests and target applications are established. A systematic basis for calculating the time interval (TI) to be followed during laboratory testing is proposed for the full-width printing (FWP) and filament printing (FP) processes. The proposed approach is verified by applying it to a high-strength, printable, fine-grained concrete. Comparative analyses of FWP and FP revealed that to test the buildability of a material for FP processes, higher velocities of the printhead should be established for laboratory tests in comparison to those needed for FWP process, providing for equal construction rates.

1. Introduction and definitions

1.1. Digital construction and requirements for fresh concrete

The processing of cementitious materials is the technological core of modern construction. Numerous new construction techniques based on digitalization and automation have been developed in recent years; see e.g. [1–6]. In this paper, authors use the generic process title Digital Construction (DC), which denotes automated additive (or generative) construction with cementitious materials. DC opens a multitude of opportunities and technological advancements:

- no need for formwork, enabling higher geometric flexibility [5,7],
- additional functionalities [1,2,5],
- considerable reductions in time and cost [8],
- low dependency on skilled labor, etc.

However, the major significance and revolutionary potential of DC reveal themselves in the context of Construction Industry 4.0. DC makes construction a fully digitalized, seamless process and represents a logical, decisive step from the already well-developed tools (CAD, BIM, etc.) of digital design and planning towards digital manufacturing.

Two common digital construction techniques are “selective material deposition by extrusion” and “selective binding”. The working principles and details of these two approaches are described in more detail in [6,9,10]. The extrusion-based techniques appear more suitable for large-scale and on-site applications. In general, the dimensions of the printing device for selective binding techniques must be bigger than those of the printed element [3,8]. This is not the case for many extrusion-based DC technologies, as demonstrated in the examples of CONPrint3D [8] and Apis Cor [11]. Furthermore, in the case of selective material deposition by extrusion, material is delivered only where it is permanently needed and should therefore be sufficiently “buildable” to retain its geometry. In contrast, in selective binding techniques, the support material surrounding the material to be bonded is crucial to maintain its shape while it is still in plastic state. The need for support material has both positive and negative consequences: structures of any geometrical shape can be produced (positive), however, all the unbinded material must be eventually removed (negative). Apparently, the selective binding processes are also more sensitive to surrounding conditions than to the selective material deposition by extrusion. Furthermore, the vertical deposition rates in selective binding techniques are constrained by the allowed low maximum thickness of individual layers. The “liquid binder” must be able to penetrate completely through the granular “dry powder” [12]. As a consequence, the thicker the granular layer the more challenging is the intrusion of binders, which are often yield-stress fluids. In the case of extrusion, the vertical deposition height is constrained by the static yield stress and the geometry of the layer/element. In addition, since the material is deposited only on the element geometry layout, the overall execution times are shorter [12] than in case of selective binding. Thus, at this stage the application of selective binding techniques seems to be more practical

* Corresponding author.
E-mail address: nerella@msx.tu-dresden.de (V.N. Nerella).

https://doi.org/10.1016/j.autcon.2019.102986
Received 17 August 2018; Received in revised form 1 October 2019; Accepted 12 October 2019

a) b) c)

Fig. 1. a) CONPrint3D technology as example of full-width printing [courtesy: Chair of Construction Machines, TU Dresden], b) Contour Crafting as example of filament printing [courtesy: Contour Crafting], c) Wonder Bench at Loughborough University as example of fine filament printing (photo by V. Mechtcherine).

for only off-site production of complex elements having relatively small dimensions. This is one reason why this article focuses exclusively on extrusion-based techniques. Another reason is that due to the mandatory presence of support material, buildability is not a primary challenge in the context of selective binding technology.

For the purpose of this study, the authors distinguish between full-width printing (FWP) and filament printing (FP) based on their layering techniques. In FWP the breadth/width of the extrudate is equal to that of the target element, as in CONPrint3D; see Fig. 1a. In case of FP the breadth of the extrudate is many times smaller than the breadth of the target element, as in Contour Crafting [1,2,4] (see Fig. 1b) or even more pronounced in fine filament approach called Concrete Printing [2,13,14]; see Fig. 1c. Consequently, the general cross-sections of FP elements consist of outer layers (shell/mold) and inner layers/fillings.

The primary requirements of cementitious materials for selective material deposition by extrusion, in terms of engineering properties, are: 1) pumpability, 2) extrudability and 3) buildability; see also Fig. 2. Adequate pumpability should ensure the uninterrupted transportation of fresh concrete and depends on, among other parameters, the plastic viscosity of the concrete or the formation of lubricating layer [15,16]. Extrudability refers to the ease of continuously extruding a material at a given flow rate; it depends on the rheological properties of the fresh concrete and the geometrical configuration of the extruder or printhead [17]. Buildability, the term and the central subject of this article, is defined as *the ability of an extruded cementitious material to retain its geometry (shape and size) under sustained and increasing loads in fresh or transient state*. This definition relates closely to the statement by Le et al. [14] "the printed filaments should be formed with minimal deformation under the weight of subsequent layers". Alternatively, Lim et al. [18] defined buildability as "the resistance of deposited wet material to deformation under load". Kazemian et al. [19] defined shape stability as "the ability to resist deformations during layer-wise concrete construction" and specified "three main sources of deformation: self-weight, weight of following layers, and extrusion pressure".

As pointed out in [8], DC is a process of many dualities, e.g. the duality of pumpability and buildability. The rheological properties favorable for pumpability and buildability differ markedly. Similar duality arises while determining the 'rate of printing', which effects economic efficiency, possible formation of "cold joints", etc. From a scientific perspective, the rheological properties of fresh cementitious material are the most crucial aspect of DC, since they affect not only the process parameters but also the properties of the final product.

To fulfil the main requirements of extrusion-based DC, cementitious material should be thixotropic, quick setting, quickly hydrating, densely packed and should possess well controlled (through internal or external triggers) rheological properties such as yield stress and plastic viscosity [20–22]. While this general approach is widely understood, many essential aspects are still under research. The open questions include the systematic choice of rheological parameters and identification of their threshold values. Most importantly, validated experimental methods are necessary to characterize and ensure the desired material properties. In their work, the authors address the question of how one of the primary engineering properties of cementitious materials for DC, namely buildability, can be systematically characterized. Specifically addressed questions are: 1) what is the representative geometry of a wall to test in lab-scale buildability tests? and 2) what is

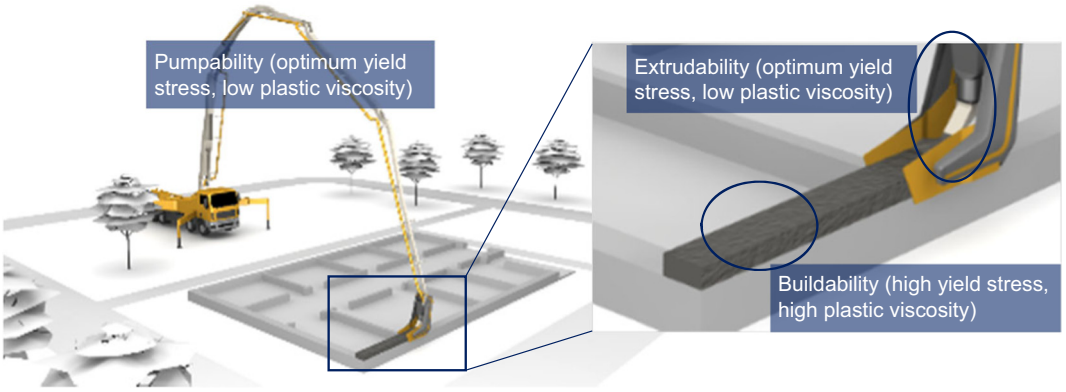

Fig. 2. Illustration of key properties for printable concrete on example of CONPrint3D technology (base sketches are of courtesy: Chair of Construction Machines, TU Dresden).

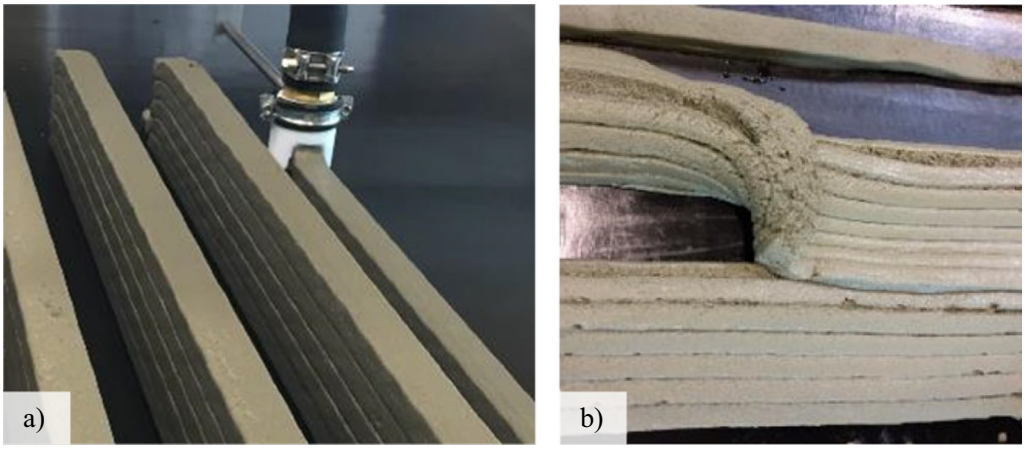

Fig. 3. a) 3D-printed fine-grained concrete specimens (up to five printed layers are depicted here, time interval was 30 s), b) a collapsed printed specimen with buildability deficiency.

the time interval in the lab-scale tests to call a material buildable?

1.2. Buildability requirements and the problem definition

Buildability is a complex and process-specific property which depends not only on material composition, but also on process parameters such as layer geometry. The 3D-printed structure will collapse if buildability, printing rate, printing pattern and other related aspects are not in harmony; see Fig. 3b. Buildability depends on, but is not identical to, the structural build-up of cement-based materials. From a practical perspective, there are three primary parameters defining any buildability tests when applied in laboratory investigations for material characterization: 1) the height of the wall to be printed, 2) the section geometry of each layer, thus, the total number of layers to be printed, and 3) the time interval (TI) between subsequent layers. The shape of the layers and that of the element (e.g. inclination) also influence buildability. However, for purposes of this article, the authors limit the scope of discussion to vertical elements with rectangular layer cross-sections.

Since many of the properties required for 3D-printable concretes need a "perfect" balance, it is essential to consider target application at all stages of material development. The buildability-defining parameters mentioned above must be carefully determined, considering various theoretical and practical aspects, before applying them in testing the applicability of particular mixtures for a target DC. 3D-printed elements should have consistent and continuous layer geometry over the entire structure. Fig. 3 shows an example of printed specimens with varying numbers of layers and buildability. It is often appealing to print 10 or 20 or as many layers as possible and then 'designate' the material as buildable. This trivial approach neither links the material's fresh properties to the target geometry nor considers the economic viability of the target application. While such an approach is still useful for relative comparison of various compositions, printing an arbitrary number of layers with an arbitrary time interval is not a reliable method in characterizing buildability. Flowable concrete with low static yield stress, extruded to wide and thin layers using a long *TI* will likely sustain deposition of a higher number of layers in comparison to a less flowable concrete that is deposited with a much higher aspect ratio $\alpha_{L,app}$ of individual layers and a short *TI*; see Section 2. Further relevant parameters are economic viability and durability of the structure, both dependent on *TI*. Durability is a function of the quality of interlayer joints, which very importantly depends on *TI*. Thus, it is crucial to determine the buildability test parameters based on the intended application and estimated process parameters.

To the best of the author's knowledge, the paper at hand is the first paper linking economic viability to material characterization with clear specifications of "man-hour, material and machine costs" and their sources. So far, apparently exaggerated claims were made by 3D-concrete printing start-ups, for example:

- Win Sun claimed up to 70%, 50% and 80% reduction of construction time, materials and labor, respectively [23]. Further, they have claimed the construction of houses at a cost of 24 USD/m^2.
- Apis Cor has claimed construction of a house at a cost of 223 USD/m^2.

Bos et al. [24] underlined the potential of DC by noting that scaffolding and mold costs in the construction sector account for 50% of concrete construction costs. Gosselin et al. [5] stated that "3D printing is a disruptive technology which offers novel solutions that reconcile non-standard shapes, and low costs". García de Soto et al. [25] reported that significant economic benefit can be achieved by using DC for complex structures. De Schutter et al. [26] presented a perspective cost structure for the DC approaches, which consisted of labor, material, machine and design-plus-planning costs. Wu et al. [27] argued that the cost of DC should also include the cost of 3D-printers (i.e. machinery). They also emphasized that despite the claims of reduction of costs in DC, the matter remained unclear. Further, numerous scientific articles [5,20,22,28–31] have professed cost reductions with DC, nevertheless without presenting a reproducible method of cost estimation. The authors concur with the general understanding that DC will reduce total construction costs due to the absence of formwork and due to faster construction rates, etc. However, quantitative approaches are still missing. The paper represents a first attempt towards a systematic yet comprehensible (for common practitioners) cost-calculation approach for both DC research and industry.

In Section 2, previously proposed approaches to estimate buildability based on rheological modelling are critically presented before our own practice-oriented approach is introduced, which define buildability in terms of target application and process parameters. The applicability of the proposed methodology is demonstrated on an example DC process; see Section 3. Since buildability requirements depend also on the applied printing approach, a corresponding comparative analysis is presented in Section 4.

2. Determining buildability test parameters considering target application

2.1. Previous approaches

Le et al. [14] stated that buildability relates "to the capacity to print a certain number of layers or height". They have quantified buildability

as the “number of filament layers which could be built up … without noticeable deformation of lower layers” [14]. Furthermore, the authors suggested a shear strength (maximum torque measured with a vane rheometer) range of 0.3 to 0.9 kPa, which leads to the successful printing of a certain number of layers without deformation and extrudability issues. Di Carlo [32] qualitatively tested shape stability by loading cylindrical specimens in the “fresh” state using a container filled with sand. In their work Kazemian et al. [19] proposed a cylinder stability test for quick comparative evaluation of compositions' influence on buildability. They also proposed the layer settlement test in which “layers are printed on top of each other with same mechanism as full-scale printer” and suggested using that test for deciding on “acceptance” or “rejection” of a mixture. In general, two to five layers were printed and the resulting deformations were measured to evaluate buildability. Panda et al. [33] investigated the influence of the “deposition height or nozzle standoff distance” on the interlayer bond strength. In relation to buildability, they concluded that if the deposition height is reduced, the dimensional accuracy of printing is negatively affected while the interface bond-strength is increased [33].

Buildability criteria based on fundamental rheological properties [34], e.g. static yield stress, and the associated changes over time are still in their genesis; it will take some years until development and validation are complete. Generic rheological models, which can consider various process techniques, the shape of the extrudate, and the effects of temperature and other surrounding conditions will take even longer to be formulated and proven. In addition, previous approaches for buildability do not consider the economic viability of the target application. This means, even if a material is proven buildable at a particular printing rate, it is not known how the use of that particular material and/or printing rate influences the total economic viability of the target project. Hence, simple, practice-oriented, yet rational buildability-assurance criteria are necessary to accelerate the implementation of digital technologies in construction practice. One such approach is presented in the following sections. It is noteworthy here that in most practical cases a perfectly rigid layer is not necessary; a layer which deforms within the tolerances allowed is acceptable and is expected to yield a better inter-layer bond.

In their commendable work, Perrot et al. [35] considered the following primary criterion: “the flow resistance of a substrate-layer should always be higher than the vertical loads acting on top of it”. The researchers expressed the vertical loads in terms of printing speed and hydrostatic pressure of concrete. The flow resistance of the substrate-layer was expressed as time-dependent static yield stress and described by Roussel's linear [36] or Perrot's exponential evolution model for thixotropy [37].

Thus, Perrot et al. [35] proposed a critical failure time t_f to predict at what time after deposition the concrete specimen fails/fractures if vertical load is increased at rate R and the initial (when resting time is *zero*) static yield stress $\tau_{0,\ 0}$ is evolving linearly [36] with a constant slope A_{thix}.:

$$t_f = \frac{\tau_{0,0}}{\frac{\rho \cdot g \cdot R}{\alpha_{geom}} - A_{thix}} \tag{1}$$

where α_{geom} is a parameter which depends on the geometry of the deposited layer/printed element [35]. Similar to Perrot et al., Wangler et al. [20] determined the minimum time to print a layer $t_{h,\ min}$, following von Mieses criteria. In other words, the minimum time $t_{h,\ min}$ for producing a layer can also be termed as the minimum interval between two successive layers needed to ensure “buildability”.

Even though both of these [20,35] works are outstanding contributions to the subject of this paper, there are still a few challenges to be mastered before these criteria can become widely applicable. For instance, the parameter α_{geom} is not generically defined yet. Perrot et al. [35] computed α_{geom} from the squeeze flow theory of plastics. Weng et al. [38] studied the influence of sand gradation on buildability following the Fuller-Thompson theory and Marson-Percy model. They examined the buildability by direct printing tests and used the number of layers as a measure of buildability. The geometric factor used by Perrot et al. [35] and Roussel and Lanos [39] is only applicable for solid cylindrical columns. Thus, Weng et al. [38] derived a new and complex equation for hollow cylindrical columns. Geometric factors for rectangular cross-sections, let alone for irregularly shaped cross-sections, have not been published yet.

Determining the structuration parameter A_{thix} is also not a trivial task. Currently there are neither standard devices nor standard protocols for characterizing A_{thix} of cementitious materials. Even using most modern rheometers different A_{thix} values may be derived for the same material when different measuring protocols are employed. This implies that for the same material, different critical failure time or minimum time intervals can be computed using Eq. (1).

More recently, Wolfs et al. [40] developed and validated a numerical model for predicting the failure of 3D-printed concrete. Attributing the early strength (0 to 90 min) of printed concrete to “combined inter particle friction and cohesion”, they have adopted Mohr-Coulomb failure criteria, also considering time-dependency [40]. Most importantly, Wolfs et al. [40] showed that the buildability failure of printed elements occurs due to the combined effects of buckling and (plastic) yielding, usually with the former preceding the latter. The model as developed accounts for both bucking and yielding by taking a time-resolved elastic modulus E(t), Poisson's ratio v(t), cohesion C(t), angle of internal friction φ(t), and dilatancy angle ψ(t) into consideration. This model does not require the measurement of A_{thix} and computation of α_{geom} as in the above-described rheology-based model and also offers a more comprehensive prediction approach. *Furthermore, the experimental validation of the numerical model showed good qualitative and acceptable quantitative* correlations. This approach, however, requires extensive experimental studies and, similar to rheology-based approaches, high precision in execution. In addition, the approach did not address the economic viability of the target application. A simple, practice-oriented methodology for buildability tests has yet to be reported. Note that an extensive review of buildability testing approaches is not the scope of the paper at hand.

Process-induced changes in rheological properties is another crucial subject. For example, differences in values of yield stress and plastic viscosity of SCC before pumping and after pumping were recorded [41]. The variation in rheological properties may result from the “higher shear rates leading to the dispersion of cement particles and depending on available residual superplasticizer in the mixing water” [41]. Even though concrete is generally not pumped over large distances when it comes to laboratory scale extrusion based 3D-printing, it undergoes high shear rates and is subjected to high pressure in the extruder. Therefore, the exact rheological state of the extrudate may vary depending on the specific extruder and printing-circuit (mixing-transporting-extruding). If large-scale, on-site applications are realized, a pronounced influence of process/pumping on the material rheological state is to be expected. Since rheological properties are usually measured on material taken immediately after mixing, variations of these off-line measured properties in comparison to the actual extrudate rheological properties are inherent. This, however, can be solved by carrying out extensive experimental studies and by the fitting of theoretically predicted “buildability” and experimentally observed “buildability”. To the best of the authors' knowledge, no such studies have been reported yet.

2.2. Suggested approach

The first step in the proposed approach is to identify and define the target application. Thereafter, a detailed printing scenario must be established based on the building design and project planning. This task is normally seen as part of the ‘design and process’ aspect of DC work flow. Generally, it involves ‘slicing’ the 3D geometry, identifying

Table 1
Aspect ratios of various elements produced by means of digital construction.

Element	Variables	Aspect ratio	Eq. Nr.
Target wall	H_{app} = height and B_{app} = breadth/width	$\alpha_{app} = H_{app} / B_{app}$	Eq. (2)
Experimental specimen	H_{exp} = height and B_{exp} = breadth	$\alpha_{exp} = H_{exp} / B_{exp}$	Eq. (3)
Target layer	$H_{L,app}$ = height and $B_{L,app}$ = breadth	$\alpha_{L,app} = H_{L,app} / B_{L,app}$	Eq. (4)
Experimental layer	$H_{L,exp}$ = height and $B_{L,exp}$ = breadth	$\alpha_{L,exp} = H_{L,exp} / B_{L,exp}$	Eq. (5)

optimum travel route of the printhead, and determining layer breadth/width, height, and contours. In the case of massive full-width printing (FWP) such as with the CONPrint3D approach [8], layer breadth is equal to final breadth of the wall to be printed; see Fig. 1a. The methodology presented below is for full-width layer printing. Methodology for filament printing such as the case with Contour Crafting [1] is addressed in Section 4; see Fig. 1b.

For the convenience of further discussion in this article, various relevant aspect ratios are listed in Table 1.

If the height and breadth of the wall to be printed (part of the target structure) are H_{app} and B_{app}, respectively, then the aspect ratio of the continuously produced "target" element, whose buildability has to be ensured, can be expressed as:

$$\alpha_{app} = \frac{H_{app}}{B_{app}} \tag{6}$$

A straightforward but often economically unfeasible manner in verifying buildability is to produce a full-scale structure of the targeted application. Alternatively, buildability can be tested by producing a scaled-down version of the target structure in a laboratory with an appropriate 3D-printing device. However, printing an arbitrary number of layers with an arbitrary time interval will not prove a material buildable; see also Section 1.2. Thus, the authors propose calculating the minimum height $H_{min,\ exp}$ of the wall to be tested in the laboratory, using the breadth of the layers printed in laboratory experiments B_{exp} and target structure's aspect ratio α_{app} (Eq. (6)) as:

$$H_{min,exp} = B_{exp} \bullet \alpha_{app} \tag{7}$$

If the height of a single layer printed in laboratory experiments is $h_{layer,exp}$.

the total number of layers to be printed

$$n_{layers} = \frac{H_{min,exp}}{h_{layer,exp}} \tag{8}$$

Combining, Eq. (7) and Eq. 8 give:

$$n_{layers} = \frac{\alpha_{app} \bullet B_{exp}}{h_{layer,exp}} \tag{9}$$

When downscaling the wall geometry to a laboratory specimen, the limits given by each particular concrete composition must be considered. Specifically, the maximum aggregate of mixtures poses a requirement of minimum breadth and height of each single layer. Choosing the minimum dimension of layer cross-section to be three times the maximum aggregate size seems to be adequate here. Such a ratio ensures that no pronounced wall effects occur so that the features of the material do not change and the material can be well extruded. Further comments on downscaling, including possible changes in maximum aggregate size, follow in Section 2.3.

The next open question revolves around determining the time interval between layers, which depends on the rate of printing. Rate of printing is a very crucial parameter for formwork-free construction with time-dependent materials such as concrete. If the rate of printing is too high, the printed concrete may not have sufficient time for structural build-up [20,35] and hence cannot retain its shape and size. If rate of printing is too low, total construction time and costs might become unfeasible. This issue can be circumvented by printing horizontally longer layers, i.e. long travel path for the printhead in completing one layer. By doing so, the overall volumetric construction rate (combining horizontal and vertical growth of the printed structure) can still be kept high. However, lower **vertical** construction rates give rise to weak interface bonds between the layers [33,42,43]. Tay et al. [44] reported that long layer-to-layer time intervals result in weak interface bonds despite the fact that no rheological change in the material to be deposited after a time interval was recorded. They observed that resting times of as low as 5 min lead to formation of voids at layer interfaces due to the structural build-up of already deposited/first layer [44]. Thus, longer time intervals lead to the deterioration of both mechanical properties and durability. The time interval *TI* to be followed in laboratory tests can be deduced directly from the target process parameters. The total travel length L of the printhead can be determined from the layout/floorplan of the target application; see Fig. 5. With an average (horizontal) printing velocity of V_{DC}, the minimum time interval between two layers can be expressed as:

$$TI_{min} = L / V_{DC} \tag{10}$$

In the first approximation V_{DC} is assumed constant, not accounting for a) velocity variations when printing corners, and b) the acceleration and deceleration at the beginning and the end of printing one layer, respectively. For $TI > L/V_{DC}$, the printing process has to be halted, e.g. to account for possibly insufficient buildability of the applied material, thus leading to longer construction times and losses in efficiency. For $TI < L/V_{DC}$ concrete buildability is over-engineered, i.e. more than necessary, which may affect the interlayer bond negatively, but also poses greater challenges in meeting the requirements of pumpability and extrudability. While defining *TI*, the economic viability of the target application/project must be considered as well. The corresponding process term, the average velocity V_{DC}, is already addressed in Eq. 10. It is worthy to note that for a wall of given gross dimensions, the time interval *TI* in the case of FP approaches will be higher than that for FWP approaches due to longer total travel length of the printhead. This aspect is elaborated in Section 4. For any DC approach to be economically viable, the following condition according to Eq. (11) must be fulfilled:

$$Costs_{DC} \leq Costs_{CC} \tag{11}$$

where, $Costs_{DC}$ and $Costs_{CC}$ are the total construction costs in the case of the DC approach chosen and in the case of current corresponding conventional construction (CC) approach, respectively. Authors have identified the "replacement of masonry structures for residential buildings" as an example strategic objective for CONPrint3D [8]. In such case, $Costs_{CC}$ are the current total construction costs for masonry in a unit residential building.

Expressing the costs of machine and labor as cost per unit time and material costs as cost per unit volume, the total costs can be estimated by using Eq. (12):

$$\begin{aligned}&(McCo_{DC} + LaCo_{DC}) \bullet t_{DC} + MtCo_{DC} \bullet vol_{DC} + AdCo_{DC} - Sa_{DC} \\ &\leq (McCo_{CC} + LaCo_{CC}) \bullet t_{CC} + MtCo_{CC} \bullet vol_{cc} + AdCo_{CC} - Sa_{CC}\end{aligned} \tag{12}$$

where, $McCo_{DC}$, $LaCo_{DC}$ and $McCo_{CC}$, $LaCo_{CC}$ are the machinery/equipment costs and labor costs for DC and CC, respectively; $MtCo_{DC}$, $MtCo_{CC}$ are material costs for DC and CC, respectively; $AdCo_{DC}$, $AdCo_{DC}$are additional costs for DC and CC, respectively. Additional costs

represent, among others, costs of design, control, concrete curing (more elaborate in DC than CC), additional testing, consulting fees which may be necessary in the case of DC. Sa_{DC} and Sa_{CC} are savings that are exclusive to either DC or CC, respectively. For instance, if structures are produced using high-performance concrete, then the durability of such elements can be much higher than that of, as an example, masonry. This can be translated into cost per structure or representative volume. At the same time, masonry walls can be more energy-efficient than concrete walls. Such intricacies will vary for each DC application and cannot yet be generally quantified. t_{DC} and t_{CC} are the times needed for constructing the target structures in case of DC and CC, respectively, while vol_{dc} and vol_{cc} are the total volumes of material used in case of DC and CC, respectively.

Expressing time in terms of average velocity in the case of DC and inversed construction rate RI (unit: h/m^2) in the case of CC, we obtain:

$$(McCo_{DC} + LaCo_{DC})\cdot\frac{L_t}{V_{DC}} + MtCo_{DC}\cdot vol_{DC} + AdCo_{DC} - Sa_{DC} \leq (McCo_{CC} + LaCo_{CC})\cdot(RI\cdot surface\ area) + MtCo_{CC}\cdot vol_{CC} + AdCo_{CC} - Sa_{CC} \quad (13)$$

where *surface area* is the total "one-side" surface area of the element being constructed; L_t is the total travel length of the printhead, which is assumed to be equal to the travel length for a single layer L multiplied by the total number of layers n_{layers}. The traversing of the printhead without printing, for example, to move to a new printing position are not considered. Such traverses are very specific to the target application and the related process parameters and can be added to the L_t, if known.

The net value of additional costs $AdCo_{DC}$ and savings Sa_{DC} in the case of CONPrint3D are assumed to be a lump sum of costs amounting to 10% of the total construction costs. For the masonry application no additional costs other than material, equipment and labor were considered; see Section 3.2.

The minimum average printhead velocity for an economically viable DC application, Eq. (14), can be obtained by rearranging Eq. (13):

$$V_{DC,\min} \geq \frac{(McCo_{DC} + LaCo_{DC})\cdot L_t}{0.\overline{90}\cdot((McCo_{CC} + LaCo_{CC})\cdot(RI\cdot\text{surface area}) + MtCo_{CC}\cdot vol_{CC}) - (MtCo_{DC})\cdot vol_{DC}} \quad (14)$$

Since it is known that:

- L_t is equal to the length of the layer multiplied by the total number of layers n_{layers},
- *surface area* is equal to the length of the layer multiplied by the height of the wall, and
- total material volume is the length multiplied by the height and breadth of the walls,

Eq. (14) can be transformed to Eq. (15):

$$V_{DC,\min} \geq \frac{(McCo_{DC} + LaCo_{DC})n_{\text{layers}}}{0.\overline{90}\cdot((McCo_{CC} + LaCo_{CC})\cdot(RI\cdot H_{\text{app}}) + MtCo_{CC}\cdot H_{cc}\cdot B_{cc}) - MtCo_{DC}\cdot H_{DC}\cdot B_{CC}} \quad (15)$$

where H_{CC}, B_{CC}, H_{DC}, B_{DC} are the height and breadth of the walls in case of CC and DC, respectively. While $H_{CC} = H_{DC}$ is chosen here for ease of comparison, the breadth of the layers produced in DC can be smaller than that of CC. Since materials used for DC applications are often superior to masonry in terms of mechanical performance, thinner walls produced using DC can meet the same design specifications as thicker walls produced using CC. Eqs. (14) and (15) can be adapted also to other DC applications to compute a minimum average printhead velocity that should be attained to make the DC application economically viable with respect to the fabrication process as such. Certainly, there are also other factors which may influence the economic feasibility to a great extent. Thus, in general the entire process from planning to actual construction should be evaluated. Specifically, the smooth transition from digital planning to digital fabrication seems to bring with it great technical and economic potential.

2.3. Complementary considerations

2.3.1. Scope of the proposed approach

The proposed approach is applicable if DC technology is used for construction of "common" structures such as residential buildings, offices, bridges, etc. The approach yet does not address complex and unique structures with non-standard elements and artworks; for example the 3D-printed castle by Total Kustom [45]. In the authors' opinion, cost efficiency might not be the first priority for complex and unique structures with respect to use of DC. However, for mass-produced structures such as houses, the cost efficiency is one of the key requirements [46].

While applying the proposed approach, following statements should be considered:

- The economic viability approach under consideration is independent of the presented "simple buildability" test. Therefore, it can be applied stand-alone to identify the maximum TI between the layers based on economic viability. Thus, the approach can be used with any buildability tests or numerical models ([35,40,47]). This enables determination of the minimum yield-stress and the rate of structural build-up that the concrete should have for economically viable DC.
- Provided the necessary testing equipment, skilled technicians and other resources, the fundamental approaches published in Wolfs et al. [40], Suiker et al. [47] and Perrot et al. [35] can be followed to test buildability. Since the approaches in [35,40,47] do not address economic viability, Eq. (14) or Eq. (15) proposed in this paper can be used to complement these approaches.
- The proposed approach addresses base-structure construction and not the final, ready-to-commence structure. In other words, the costs of utility installations are not considered.
- Often chemical admixtures such as accelerators are used to ensure buildability. In such cases, a very important question is: in what dosage does the admixture need to be added? The approach proposed in the article at hand will enable determination of the duration of the maximum economically viable time-interval. This helps in determining the dosage of the chemical admixture to be introduced so that the required time-interval is maintained.

2.3.2. Downscaling and surrounding conditions

The proposed approach assumes that material behavior tested on the "downscaled specimens under laboratory conditions (lab-tests)" is representative of the material behavior in "full-scale structure in real application (full-scale)". In reality differences between material behavior in the lab-tests and full-scale applications may arise, e.g. due to variation in the quality of extrusion/compaction (process-induced changes) or in the evaporation rate related to the volume of printed element.

Here it is important to emphasize that the challenge posed by some differences in lab experiments and full-scale applications is a universal issue, which is not particular to buildability tests or DC in general. Taken broadly, such issues can only be resolved by full-scale tests and direct comparison, followed by error-minimization measures. The approach proposed in this paper for laboratory tests already takes into account certain considerations in mimicking conditions under full-scale application:

a) Tests are performed in-line, i.e. they are integrated in the 3D-printing process, as opposed to offline tests where material has to be

Table 2
Dimensions of the target application and corresponding calculated parameters for buildability testing.

	Parameter	Unit	Outer	Inner	Outer2	Outer3
Application	Wall height H_{app}	m		2.500	3.000	2.500
	Wall breadth B_{app}	m	0.240	0.175		0.240
	Aspect ratio α_{app}		10.417	14.286	12.500	10.417
Lab	Layer breadth $B_{L,exp}$	m			0.030	0.060
($\alpha_{exp} = \alpha_{app}$)	Layer height $H_{L,exp}$	m	0.017			0.020
	Minimum height to be tested $H_{min,\ exp}$	m	0.313	0.429	0.375	0.625
	No of layers n_{layers}	#	18	21	19	31

collected separately and tested in a test device. Thus, time-dependent influences are avoided and errors due to process induced changes are minimized.

b) Specimens are extruded using an extruder system similar to that foreseen in the prospective full-scale application, thus subjecting the tested material to similar shear history and degree of compaction.

c) The curing of laboratory specimens is adjusted to that planned for the full-scale application, indeed, if planned at all. If specific temperature, humidity, and wind conditions are expected for the full-scale application, the laboratory tests should be performed under similar environmental conditions if possible.

d) If admixtures are added in the printhead during full-scale applications, the same procedure should be implemented in the lab-scale 3D-printing.

Regarding change of scales, the authors do anticipate that the proposed approach withstands the change in scales barring some limitations, which need further investigation. So long as the changes are only in dimensions and not in shape of the geometry, the validity of the proposed approach can be seen as convincing. Nevertheless, a correction factor may need to be introduced to take dimensional change into account. Such factors can be identified theoretically/numerically and/or with help of full-scale validation experiments. It goes without saying that in some cases (full-scale applications are large and tall structures) downscaled experiments are the only feasible option to assess the buildability.

To extend the range of downscaling, the maximum aggregate size used in mixtures for laboratory experiments may be reduced. It seems feasible to decrease maximum aggregate size for 3D-printing in laboratory since the effect of maximum aggregate size can be relatively well estimated based on available contemporary knowledge. It is known from [20,35] that the buildability of a printed layer can be expressed in terms of, and proportionally depends on the structural build-up of concrete. Mahaut et al. [48] related the static yield stress of cementitious suspensions with coarse particles $\tau_c(\phi, t)$ to the static yield stress of the suspending cement paste $\tau_c(0, t)$, to the time t passed at rest, and to the coarse particle volume fraction ϕ; see Eq. (16). They suggested that the presence of ϕ volume fraction of coarse particles in a cement paste, will magnify its static yield stress as a function of the volume fraction of coarse particles $g(\phi)$.

$$\tau_c(\phi, t) = \tau_c(0, t) g(\phi) \tag{16}$$

$$g(\phi) = \sqrt{(1 - \phi)(1 - \phi/\phi_m)^{-2.5\phi_m}} \tag{17}$$

where ϕ_m is the maximum volume fraction.

In addition, Mahaut et al. [48] postulated that "the structuration rate A_{thix} has the same dependence on the coarse particle volume fraction as the yield stress". These findings imply that the parameters identified through a proposed approach on a concrete with finer aggregates could be applied to concrete with coarse aggregates using a factor similar to that of Eq. (17). However, this hypothesis is yet to be verified.

3. Applying proposed approach to CONPrint3D

Generalized approach proposed in Section 2, for determining buildability test parameters is applied here to an on-site concrete 3D-printing technology, CONPrint3D. On completion of this section, the specifications of buildability tests on cementitious materials applicable for CONPrint3D are clearly derived. As elaborated in Section 2, these necessary specifications are: height of the experimental wall to be printed, number of layers in this wall, and the time interval (TI) between the layers. The target full-scale implementation of CONPrint3D technology will be primarily with coarse-grained aggregates of maximum aggregate size 8 mm to 16 mm. However, the use of fine-grained concretes should not be excluded at this stage due to their advantages with respect to processing and the maturity of the required extrusion machine technology, "lightness" of the printhead, etc. In this context and as a first step, the verification presented below will consider an application case of CONPrint3D where fine-grained concrete is used.

3.1. Height of the wall specimen and number of layers to be tested

One- to multi-story residential buildings [8] make up an important segment of the primary target applications for the CONPrint3D approach. Table 2 presents exemplarily the dimensions of outer and inner walls for a single story. Also presented are the nozzle dimensions employed for the lab-scale 3D-printing testing device (3DPTD), which was designed in 2015 at the TU Dresden and has been used since then for material development. Furthermore, Table 2 presents various extra cases, namely Inner, Outer2 and Outer3. These cases provide additional information on how $H_{min,\ exp}$ and n_{layers} vary depending on wall and nozzle dimensions. $H_{min,\ exp}$ and n_{layers} are calculated using Eq. (7) and Eq. (9). These calculations highlight the consideration of layer geometry in the proposed buildability test methodology. If the laboratory nozzle breadth is increased and laboratory nozzle height remains unchanged, then the height $H_{min,\ exp}$ to be tested in the laboratory also increases. If the breadth of the target wall decreases, as in the case of inner walls, then the $H_{min,\ exp}$ increases. Similarly, if the height of the printed layer, i.e. nozzle in the lab, increases where its breadth remains unchanged, then the number of layers to be printed in the laboratory tests will decrease. These variations of buildability test specifications are crucial, considering that the nozzle dimensions in the laboratory printers may vary significantly even though the final targeted element (application) dimensions and the geometry of the real-application printhead do not change. Fig. 4 illustrates how the number of layers varies a) if nozzle height is kept constant and breadth is increased and b) breadth is kept constant and height is increased.

The material explicitly considered in this article is a high-strength, fine-grained concrete, denoted as C2. With a compressive strength at an age of 28 days exceeding 80 MPa, the concrete C2 is developed for the outer load-bearing walls of the target residential buildings. Thus, for the laboratory buildability tests, case 'Outer' presented in Table 2 will be considered. The actual nozzle height used for the experiments (see Section 3.3) is 17 mm. As shown in Table 2, to ascertain the buildability of the Mixture C2, 18 layer specimens have to be printed in the laboratory tests. The test specimens shall comply with maximum time-

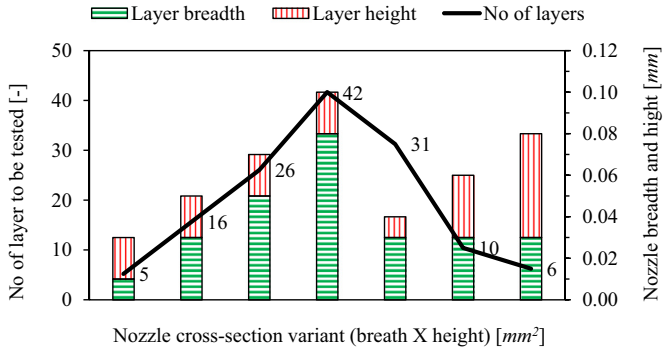

Fig. 4. Variation of number of layers to be tested with variation in nozzle cross-section for a constant target application.

interval and prescribed tolerances, for example, according to the German standard DIN 18202:2013-04 [49]. The handling of the cases other than Outer should follow the same routine; note that a perspective 20 mm nozzle height is assumed for the calculations of all cases except Outer in Table 2.

3.2. Time interval (TI)

The calculations presented below are valid for walls of one floor of a multi-story house erected using CONPrint3D. For purposes of comparison, an estimation for walls made of conventional masonry are provided too. The process parameters of masonry construction are given in Table 3; here the use of sand-lime bricks is assumed. These are used to calculate the construction costs for the masonry work and to derive $V_{DC,\min}$. The outer wall length of 43.04 m and the inner wall length of 19.86 m as presented in Table 3 are calculated from the floor layout of the target application, presented in Fig. 6. The openings (e.g. windows) are also included in the travel lengths as the printhead must traverse this distance, however, without depositing material. To calculate the printhead travel length for each layer to be deposited, it is essential to address "printing scenarios" or the aspect of "tool-path optimization". For the sake of simplicity, in the example presented here we assume that one complete layer along the outer walls is printed first. Subsequently, further layers of the outer walls are added upon one another. After the completion of the outer walls, the inner walls are produced and frictionally connected to the outer walls by stainless steel anchors, which are inserted into each layer. In contrast, to this simple scenario, the path of the printhead can be defined in numerous ways, as shown in Fig. 7, while various algorithms can be utilized for determining the optimum printing scenario. In such cases, the wall length in Table 3, must be adjusted according to the printing path finally chosen.

It is noteworthy that the choice of a suitable starting point and the minimization of *idle-traverses* (travel times without concrete discharge, shown with the dashed line in Fig. 7) are of great importance in any printing strategy.

The optimal printing path depends on numerous boundary conditions. An essential optimization criterion is the path length. While the shortest printing path should be generally preferred, it cannot always be used due to other constraints; such as the motion and clearance profiles of the printhead or on-site construction process conditions. Zhang et al. [28] adapted the so-called "traveling salesman problem (TSP)" to determine the optimal tool path for constructing with Contour Crafting technology. They derived the shortest paths by adding multiple vertices in the corners and wall connections, and then by transforming the optimization problem from the node-oriented to the edge-oriented view.

The rate at which masonry construction takes place is generally expressed in terms of the time needed to complete a square meter of a wall, usually an hour. Since this rate is inverse to the rate generally considered in concrete construction rates, i.e., unit area per unit time, more specifically square meters per hour, it is termed here *inversed rate of construction* with a notation *RI;* see Section 2. The RI values used in the article are according to *Baukosteninformationszentrum Deutscher Architektenkammern* (BKI) and for the case of masonry wall type KS-L-R 8 DF 240 mm [50]. The rate of construction is given per person. Thus, when deriving V_{DC} using Eq. (14), one must multiply *RI* with actual number of workers working on the masonry application; which is in this case is three, leading to an effective *RI* of 0.2 h/m^2.

Machine costs presented in Table 4 for a small crane (Kleinkran C.2.00.0007I) are in accordance with BGL 2015 [51]. These costs include repair, depreciation and interest costs. The material costs are also calculated for the masonry wall type Format KS-L-R 8 DF 240 mm and include delivery and mortar costs [50]. Process parameters of the CONPrint3D are presented in Table 4, which are used to calculate the construction costs and derive $V_{DC,min}$.

Since CONPrint3D is an FWP process, the breadth of the printed layer is equal to the breadth of the target wall. For the case "Outer" considered here, the breadth of a printed layer is 0.24 m. The thickness of the layer is a process parameter, which affects the total number of layers to be printed, total printing time, and thus construction costs. The maximum feasible layer thickness depends on the material properties. For the case presented here, layer thickness was assumed to be two-thirds of the layer breadth in accordance with the geometrical proportions of the nozzle of the lab printer. Numerous scaled-down wall-elements had been already printed using the aforementioned nozzle-aspect ratio. Machine costs for CONPrint3D as given in Table 4 are, at the current stage, higher than that of masonry construction. They include costs for a modified concrete boom pump, costs for transporting concrete from mixing plant to construction site and costs for adjusting and calibrating the pump on the site. In general, for DC technologies lower manpower costs are envisioned in comparison to conventional construction. In the case of CONPrint3D, two workers would be necessary from today's perspective: one for machine monitoring and one for auxiliary works. Based on BKI 2017 values, the average wage of one person is calculated at 35 € per hour [50].

The material costs for CONPrint3D, 130.00 €/m^3, are calculated conservatively for the high-strength printable concrete *C2* used in the experiments. They include material costs for admixtures and additives (micro-silica suspension, fly ash and superplasticizer). The cost of C2 is approximately 70% higher in comparison to the cost for ordinary

Table 3
Dimensions of the target application and process parameters of example masonry constructions.

	Parameter	Unit	Outer	Inner	Outer2	Outer3
Application	Wall height	m		2.500	3.000	2.500
	Wall length	m	43.040	19.860		43.040
	Wall breadth	m	0.240	0.175		0.240
Masonry	Inversed rate of construction	h/m^2				0.6
	Machine costs	€/h				14
	Labor costs per person	€/h				35
	No. of workers	person				3
	Material costs	€/m^3				164.05

Table 4
Process parameters for the application of CONPrint3D.

	Parameter	Unit	Outer	Inner	Outer2	Outer3
CONPrint3D	Layer height	m	0.160	0.117		0.160
	Layer breadth	m	0.240	0.175		0.240
	Machine costs	€/h			140	
	Labor costs (2 persons)	€/h			70	
	Material costs	€/m^3			130	

concrete of the strength class C25/30 used in conventional construction. The Mixture C2, containing expensive additives and admixtures, was chosen deliberately for the calculations to ensure process-safe implementation of the onsite digital construction of load-bearing elements. Note that printable concretes are, in general, contain fine mineral additives and chemical admixtures to achieve the required rheological, mechanical and/or durability characteristics. The fine-grained concrete considered here has a compressive strength of over 80 MPa at an age of 28 days. However, for the target residential building application, the required concrete class according to DIN EN 206–1 is C25/30. Thus, a considerable reduction in material costs is feasible in the course of the optimization process. In addition, by replacing the Portland cement used in this research with sustainable alternatives such as Limestone-calcined clay cement (LC^3), the materials costs can be further reduced [52].

In addition to material, machine and labor costs, 10% additional costs are added to the total costs of CONPrint3D as detailed in Section 2.

The minimum average printhead velocity $V_{dc,\min}$ for CONPrint3D application, to be equally economically viable with masonry construction, is calculated using Eq. (14) and data from Tables 2, 3 and 4. After knowing $V_{dc,\min}$, the maximum (again economically viable) *TI* between layers can be calculated as $TI = L_t/V_{dc,\min}$. Table 5 presents both $V_{dc,\min}$ and maximum *TI* values calculated for various cases of CONPrint3D application. For the Outer case, the time interval between extruding subsequent layers should not exceed 43.9 min. In addition to the maximum *TI,* it is also possible to define the minimum *TI* based on the maximum printing speed of the printer to be used. The current laboratory printer for CONPrint3D has $V_{dc,\max} = 540$ m/h. However for the laboratory test presented in this paper, a printhead velocity of 270 m/h was set, which is used to calculate the minimum feasible time interval as $TI = L_t/V_{dc,\max}$; *see* Table 5. The minimum *TI* for the Outer case is 9.56 min; see Table 5. It goes without saying that if printing of the entire construction were to occur at a rate close to $V_{dc,\max}$, then the costs and construction time in case of CONPrint3D will be considerably reduced in comparison to those of conventional construction.

The minimum TI variation with printing velocities is shown in Fig. 8 for printing lengths of 5 m to 100 m. The figure shows that the influence of $V_{DC,\max}$ on minimum TI is significant only below certain printhead velocities. Furthermore, the lower the printing length the lower the influence of $V_{DC,\max}$ on minimum TI.

3.3. Experimental verification

For production of the wall specimens, a custom-developed 3D-concrete-printing test device (3DPTD) was used; see Fig. 9. The 3DPTD is equipped with a progressive cavity pump (PCP) to extrude concrete. The printhead speed and the time interval between the depositions of two subsequent layers can be pre-programmed. The printhead velocity and concrete flow rate are synchronized. The synchronization schema is detailed in [17]. The PCP used in the 3DPTD can rotate at 15–150 rpm, delivering up to 4 L/min concrete, varying according to rheological properties [17]. The maximum pumping distance with an operating pressure of 20 bar is 15 m. The concrete container has a capacity of 50 L. Fine-grained concretes with a maximum aggregate size of 3 mm can be pumped and extruded. The entire printhead when filled with concrete weighs under 150 kg and is traversed in 3 dimensions. A 3D-printed nozzle with a rectangular outlet of breadth 30 mm and height 17 mm was used in this study.

Table 5
Process parameters of an example CONPrint3D application.

Parameter	Unit	Outer	Inner	Outer2	Outer3
$V_{dc,\min}$	m/h	58.9	72.0	50.0	100.1
Maximum *TI*	min	43.9	16.5	51.6	51.6
$V_{dc,\max}$	m/h				270.0
Minimum *TI*	min	9.6	4.4		9.6

The buildability of a fine-grained concrete C2 (see Fig. 9c) was verified using the approach proposed above. The target application considered is a residential house; see Section 3.1 and Fig. 5. Specifically, for the case Outer; see Tables 3 to 5.

The design of the buildability experiment is to produce a given number of layers n_{layers} with a defined time interval *TI* between layers. If the printed wall retains its geometry and dimensions, then the tested material is applicable for the target application. As determined in Sections 3.1 and 3.2, a total of 18 layers with maximum time intervals of 43.9 min must be printed. The time interval mentioned here is the upper limit. *TI* longer than 43.9 min adversely affects economic viability, if all other parameters are assumed constant. It is noteworthy that such “long” time intervals may reduce inter-layer bond strengths. Hence, while developing printable concretes, interface properties [33,42,43] and extrudability [17] must be considered as well. The composition C2 was investigated for interface bond strength using macroscopic, microscopic, and neutron radiography techniques. Results of those studies were published by authors in [53,54]. The short, 2 min TI proved to yield printed structures with minimal anisotropy. Considering this, it was decided to assess the buildability using a rather short TI of 2 min.

At a concrete age of 20 min from water addition, printing experiments were started. The primary wall (Wall 1) consisted of 25 layers, which were printed at a constant velocity of 75 mm/s and time intervals of 2 min. Note that at least 18 layers must be printed with the developed concrete to “pass” the buildability test. Upon observing no visual deformation of the layers after completion of 18 layers, additional 7 layers were printed. Since, more than the required 18 layers could be printed with a TI much shorter than the economically required TI, the Mixture C2 could be designated “buildable” for the considered application case. Furthermore, the dimensions of the wall specimen were measured at an age of 1 day with a precision of 0.1 mm. Note that printed individual layers' cross-sectional dimensions can vary from those of the nozzle outlet; not only depending on the buildability but also on the flowrate of the material. To objectively distinguish the deformation due to weight of upper layers from the deviations due to excessive material pumping, a separate reference wall was also printed with the same printing speed but with only three layers. Following specific metrics were observed for both walls (“Wall 1” and reference wall “Wall Ref”):

a) Visually detectable deformations;
b) Height of the printed wall;
c) Δ_{dpt} = (breadth of the bottom layer − breadth of the top layer) / breadth of the top layer.

The results of these measurements are presented in Table 6. No visual collapse or deformations of the layers could be noticed on the printed specimens. When seen from top-view, all layers appeared consistent and no bulging of lower layers could be detected; see Fig. 10b. The wall surface looked flat with right-angled layer corners. The height of Wall 1 with 25 layers was only 0.3 mm lower than the designed height of 425 mm. This asserts the buildability of Mixture C2.

Thickness of the layers was measured along the length at each 10 cm. From these measurements the average thickness values were calculated. Every time the printhead accelerated from rest to 75 mm/s and every time it decelerated from 75 mm/s to zero velocity, minor disharmony occurred in the proportionality of the concrete flowrate and printhead velocity. Thus, the thickness measurements were only considered starting 10 cm away from the edges. The mean breadth of the reference wall's top and bottom layers were 32.3 and 32.1 mm, respectively. The observed, maximum 2 mm, deviation from the designed 30 mm nozzle width does not necessarily is due to the deformation of the printed layers. For the Wall Ref (three printed layers

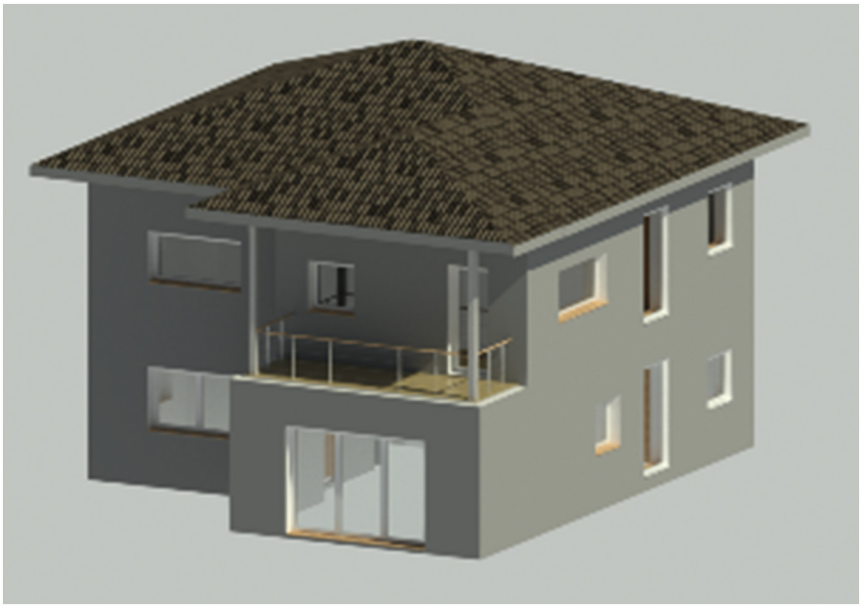

Fig. 5. Sketch of a representative target residential building.

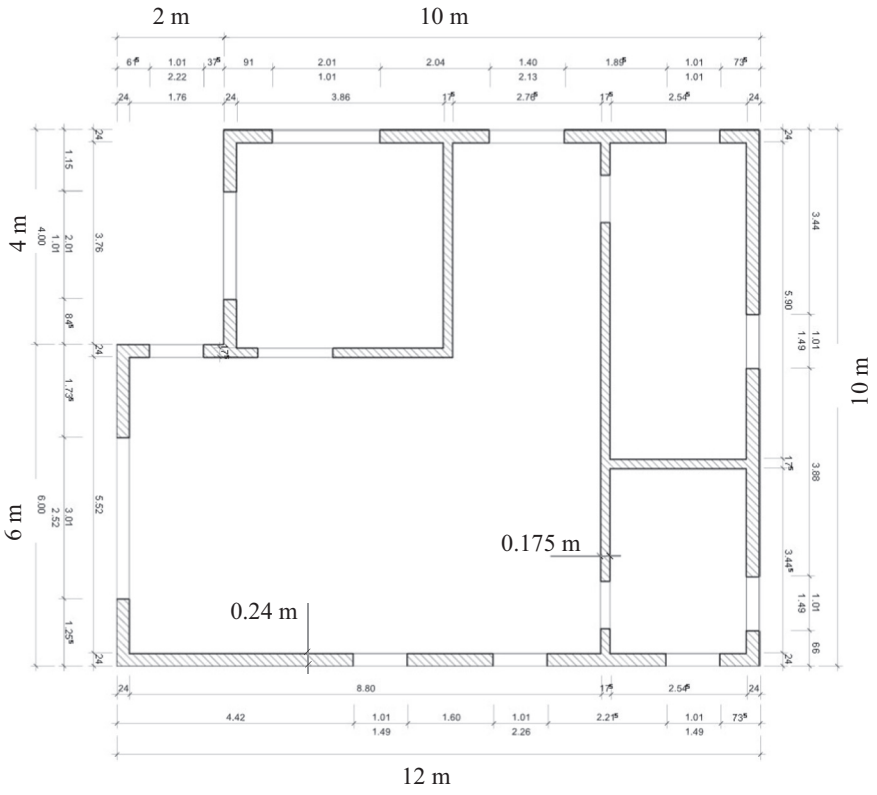

Fig. 6. Layout and dimensions of a storey of the target house.

only), the breadth of the layers was also up to 2 mm higher than the nozzle breadth. If the deviation from the nozzle geometry would be due to material deformations under load, then in the case of Wall 1 (25 layers) such deformations must be considerably higher than those of Wall Ref. This observation confirms that the measured deviations were not due to the layer deformations under load of subsequent layers. Moreover, if the printed layers would have deformed due to the weight of upper layers then the breadth of the bottom layer should be wider than that of the top layer. The Δ_{dpt} values are 0.0 in both walls, indicating no significant differences in the breadth of the top and bottom layers. The minor deviations from the nozzle breadth are attributed to the fact that pumping had slightly higher material flowrate than need to deliver the required volume for printing the cross-section of 30 mm by 17 mm.

Overall, the visual observations as well as height and breadth measurements confirm the stability and the buildability of Mixture C2 up to 25 layers with a TI of 2 min.

For further studies, the use of process monitoring techniques such as the ones proposed by Kazemian et al. [19], Wolfs et al. [40] or Buswell et al. [6] is suggested. In general, continuous measurement of layer

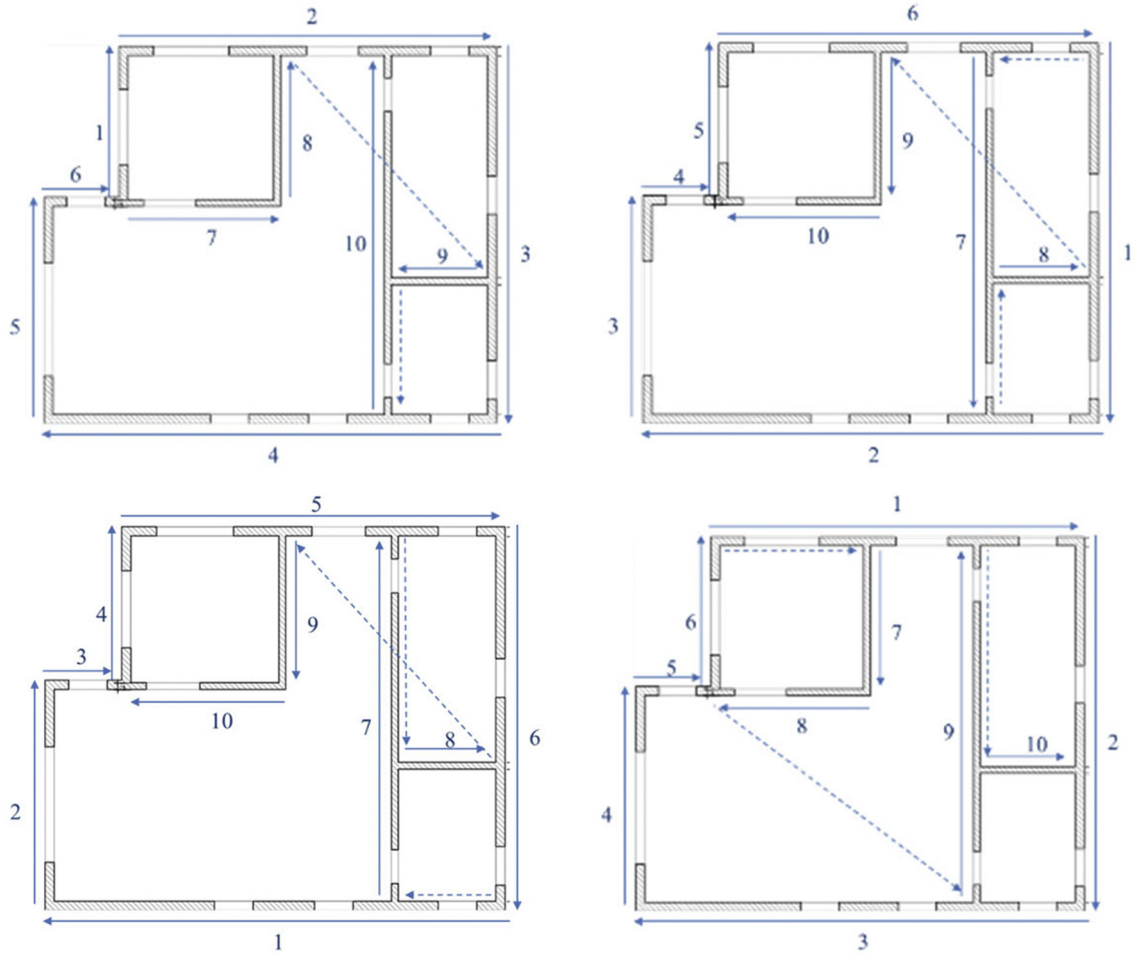

Fig. 7. Various scenarios for printing the walls of a house considered under consideration. Full lines indicate printing and dashed lines indicated traversing without extruding concrete.

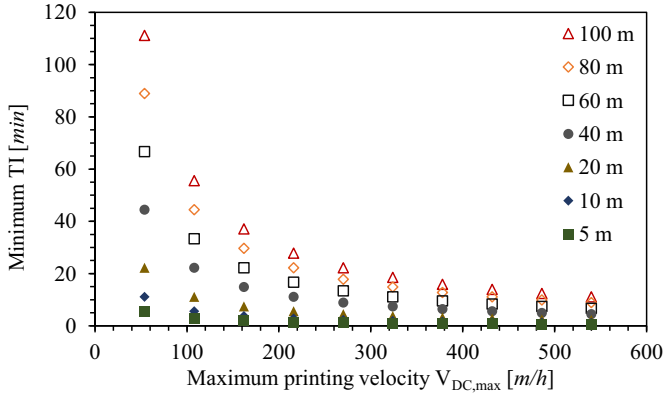

Fig. 8. Variation of minimum TI with maximum printing velocity (shown for printing lengths of 5 m to 100 m).

deformation with optical sensors or by image recording and analysis enables precise assessment of layer deformation during printing. Since the developed material could pass the buildability test with a much shorter TI than the calculated maximum TI, further optimization of the mixture can be generally carried out. A less buildable mixture with, likely, lower cement, additives and admixtures contents could be composed. However, in such cases the effects of changes in the composition on pumpability, extrudability and anisotropy (weak interfaces) must also be considered.

4. Buildability requirements for filament printing and full-width printing

The 'height' component of the buildability test parameters remains essentially the same for both the full-width printing (FWP) and filament printing (FP) approaches. In contrast, the 'effective length' of each layer to be printed varies significantly between FWP and FP, which directly affects the *TI*. The 'effective length' refers to total travel distance, which is often greater than the length of the actual wall. The printhead with a single-nozzle opening (as in [2,4,8,11]) travels approximately twice the distance in case of FP when compared to FWP, to complete the deposition of the outer filaments; see Fig. 11. Furthermore, additional time is needed to place the inner wave-like filament. Consider V as the velocity of the printhead that is calculated using distance traversed and $V_{effective}$ as element horizontal printing velocity that is calculated using printhead displacement. In the case of full-width printing the entire layer cross-section is printed in one run. Thus, the printhead velocity $V_{printhead,FWP}$ is equal to the "effective" horizontal printing velocity $V_{effective,FWP}$. For FP, $V_{printhead,FP}$ is lower than the $V_{effective,FP}$. Consequently, to achieve an equal construction rate in the case of FP, printhead velocity $V_{printhead,FP}$ has to be much higher than in the case of FWP. A simplistic approximation for FP can be:

$$V_{printhead,FP} = V_{effective,FP}\,(2 + \mathrm{k}) \text{ with } \mathrm{k} = \mathrm{f}(\lambda, \hat{u}) \tag{18}$$

with λ is the wavelength and $\hat{u}$ is the amplitude of the wave depicting the inner filament of the wall produced by means of FP; see Fig. 11c.

Since the $V_{effective}$ of FP is much lower than that of FWP the *TI*

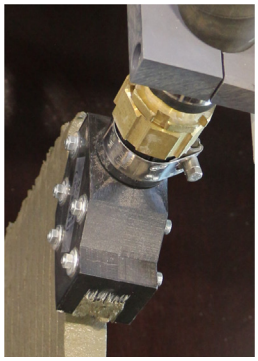

Constituent	Dosage (kg/m^3)
Cement	391
Micro-silica suspension (50% water)	213
Fly ash	213
Sand 0.06-2 mm	1260
Water	138
PCE	11

a) b) c)

Fig. 9. a) Printhead of 3D-printing test device, b) nozzle and c) printable concrete composition C2.

a) b) c)

Fig. 10. 700 mm-length wall specimen (Wall 1) printed with time intervals of 2 min between layers. Photos are taken after printing 23 layers; see Table 6 for dimensions. The length of the ruler in a) is 30 cm.

between layers in case of FP is also longer. Although it may appear advantageous in terms of "available" resting time for structural build-up, a longer *TI* means a reduction in the economic viability and a higher risk of formation of weak interface bonds between layers. Savings in material through FP in comparison to FWP are less significant: as Tables 3 and 4 show, material costs are not the major contributors for the total construction costs.

Eq. (18) implies two cases that are summarized in Table 7, where FP is compared to FWP for the same target application.

It is of interest mathematically to describe the above-mentioned intricacies of buildability requirements for FP and FWP in order to facilitate:

- choice between FP and FWP, if the choice of material is restricted;
- extension of the model presented in Section 2 to FP cases by providing a mathematical description of *TI* in terms of wall geometry. For instance, the minimum *TI* in the case of FP can be calculated using Eqs. (28)–(30);
- Development of process-agnostic, printable concretes, i.e. concretes applicable for both FP and FWP processes.

The following is the derivation for the needed $V_{printhead,FP}$ in relation to $V_{printhead,FWP}$, provided only one nozzle is used and constant economic viability or constant construction rate is to be achieved (Case 1 in Table 7).

Assuming

- length of the wall to be produced: L,
- distance that the printhead travels in case of FWP (Fig. 11a): $L1$,
- distances that printhead travels in case of FP (Fig. 11b, -c): $L2$ for outer and $L3$ for inner profile,

we obtain:

time for printhead travel in FWP: $t_{FWP} = L1/V_{printhead,FWP} = L1/V_{effective,FWP}$ and

time for printhead travel in FP: $t_{FP} = (L2 + L2 + L3) / V_{printhead,FP}$.

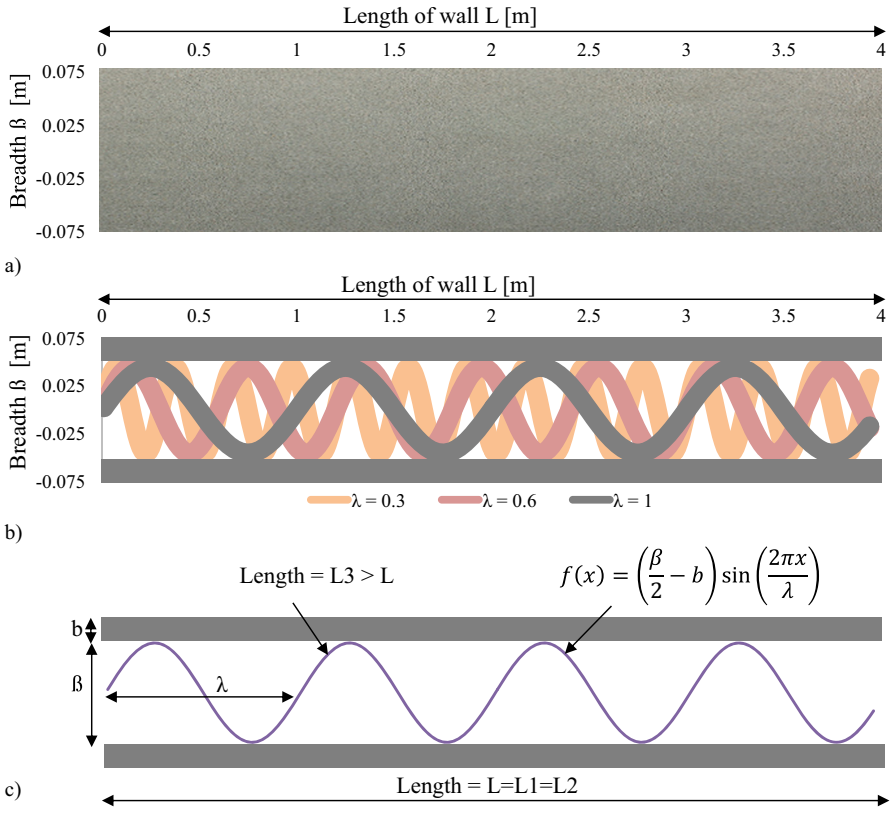

Fig. 11. Schematic top sectional views of two walls of identical length and width, produced through a) full-width-printing FWP) and b) filament-printing FP. The FP figure also illustrates two additional alternatives for inner filament defined by wavelengths λ. c) A scheme showing wavelength and semi-amplitude of sinusoid depicting inner filament in FP.

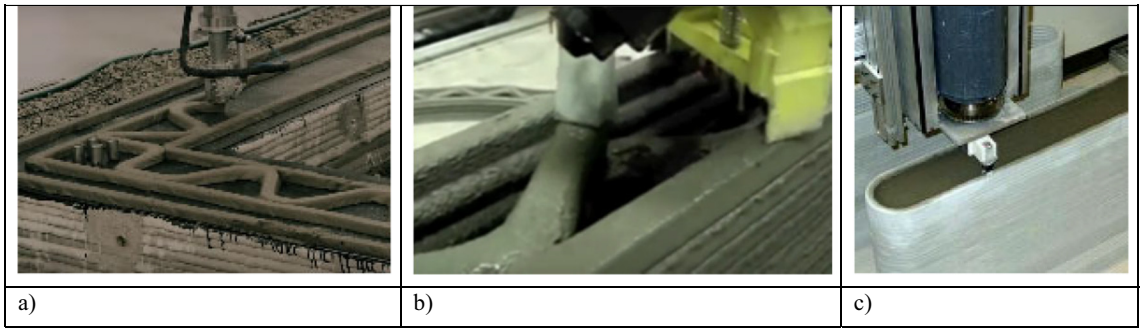

Fig. 12. Various scenarios for printing "one set of horizontal layers" in case of FP printing process: a) single nozzle – three passes are needed [11], b) three nozzles – two passes are needed [55] and c) representation of single nozzle with "post-filling" of the empty space between layers [56].

Assuming equal economic viability in FP and FWP as in Case 1 (Table 5), both the times should be equal:

$$\frac{L1}{V_{effective},\ FWP} = \frac{L2 + L2 + L3}{V_{printhead,FP}} \tag{19}$$

$$V_{printhead,FP} = \left(\frac{L2 + L2 + L3}{L1}\right) V_{effective,FWP} \tag{20}$$

Since the length of the wall $L = L1 = L2 \neq L3$ (21)

$$V_{printhead,FP} = \left(2 + \frac{L3}{L}\right) V_{effective,FWP} \tag{22}$$

Expressing the inner filament in FP as a sinusoid $y = i \sin jx$ from 0 to L; the length (distance between 0 and L) of the inner filament is:

$$L3 = \int_0^L \sqrt{1 + ((i * j\cos^2 j\times dx} \tag{23}$$

In Eq. (23), i = semi-amplitude of the inner filament = $\hat{U} = ß/2 - b$ and $j = 2\Pi/\lambda$.

with $ß$ and b are the breadth of the produced wall and filament,

Table 6
Dimensions of the specimens produced for buildability tests.

Wall	No of layers	Height [mm]	Std. dev.	Breadth top [mm]	Std. dev.	Breadth bottom [mm]	Std. dev.	Δ_{dpt}
1	25	424.7	0.7	32.3	0.1	32.1	0.3	0.0
Ref	3	50.5	0.0	31.9	0.3	32.4	0.2	0.0

Table 7
Requirements in case of FP depending on the comparative constant.

	Comparative cases of FP and FWP	FP requires
1	Constant economic viability	• Higher $V_{printhead,FP}$ • More sophisticated 3D-printer setup to handle the higher mechanical stresses induced by faster accelerations and deceleration of the printhead
2	Constant printhead speed $V_{printhead}$	• Lower buildability (*TI* will be higher) • higher open-time/working-window of the construction material • Longer construction times

respectively, and λ is the wavelength of the inner filament; see Fig. 11c.

The length of the inner filament expressed in sinusoid attributes can be calculated according to Eq. 24:

$$L3 = \int_0^L \sqrt{1 + \left(\left(\frac{\beta}{2} - b\right) * \frac{2\pi}{\lambda}\right)\cos^2\frac{2\pi x}{\lambda}}\, dx \tag{24}$$

From Eqs. (22) and (24):

$$V_{printhead,FP} = \left(2 + \frac{\int_0^L \sqrt{1 + \left(\left(\frac{ß}{2} - b\right) * \frac{2\pi}{\lambda}\right)cos^2\frac{2\pi x}{\lambda}}\, dx}{L}\right) V_{effective,FWP} \tag{25}$$

Eq. 25 enables determination of printhead velocity to be followed while applying FP to retain economic viability equal to that of FWP processes.

Furthermore, if equal economic viability is not the primary concern and constant printhead speed is followed for both FP and FWP, i.e. Case 2 in Table 7, then a higher minimum *TI* is valid for FP. The following relationship between $TI_{min,FP}$ and TI_{minFWP} can be obtained:

$$TI_{\min,FP} = \left(\frac{\text{Travel length in case of FP}}{\text{Travel length in case of FWP}}\right) TI_{\min,FWP} \tag{26}$$

$$TI_{\min,FP} = \left(2 + \frac{\int_0^L \sqrt{1 + \left(\left(\frac{ß}{2} - b\right) * \frac{2\pi}{\lambda}\right)cos^2\frac{2\pi x}{\lambda}}\, dx}{L}\right) TI_{\min,FWP} \tag{27}$$

In addition, with no comparison to FWP, the minimum *TI* in case of FP can be calculated for a printhead velocity of $V_{printhead}$:

$$TI_{\min,FP} = \frac{2L + \int_0^L \sqrt{1 + \left(\left(\frac{ß}{2} - b\right) * \frac{2\pi}{\lambda}\right)\cos^2\frac{2\pi x}{\lambda}}\, dx}{V_{printhead}} \tag{28}$$

Eq. (28) is a generalized formula to determine the minimum time intervals between layers, which must be followed during laboratory buildability tests if an element of target length L is produced through FP.

It must be noted that Eq. (28) is valid only if one nozzle is used to print the filaments; see Fig. 12a. If a printhead with more than one nozzle is used for printing, then the following scenarios can be followed:

a) Two passes are needed for one horizontal layer of the target wall. In the first pass, two nozzles extrude the outer 'shells' and in the second pass, one nozzle extrudes the inner 'wave'; see Fig. 12b. An example of this scenario is demonstrated by Contour Crafting [55];
b) One pass is needed for one horizontal layer of target wall. Two nozzles extrude the outer 'shells' and in parallel, a third nozzle prints the inner 'wave'. To the best of authors' knowledge, this scenario has not yet been demonstrated.

Moreover, in both scenarios one additional pass of the printhead or other device will be needed if spaces between 'shells' and 'wave' need to be filled, e.g. with insulating materials or (self-compacting) concrete; see Fig. 12c.

For the scenarios 'a' and 'b' mentioned above, Eq. (28) can be transformed to Eq. (29) and Eq. (30), respectively:

$$V_{printhead,FP} = \left(1 + \frac{\int_0^L \sqrt{1 + \left(\left(\frac{ß}{2} - b\right) * \frac{2\pi}{\lambda}\right)cos^2\frac{2\pi x}{\lambda}}\, dx}{L}\right) V_{effective,FWP} \tag{29}$$

$$V_{printhead,FP} = \left(\frac{\int_0^L \sqrt{1 + \left(\left(\frac{ß}{2} - b\right) * \frac{2\pi}{\lambda}\right)cos^2\frac{2\pi x}{\lambda}}\, dx}{L}\right) V_{effective,FWP} \tag{30}$$

Similarly, Eq. (28) can be reformulated according to the number of nozzles/robots used. As can be seen in Eq. (30), even if three nozzles are used and moved at the same speed as in case of FWP, the effective printing velocity in case of FP will be lower in comparison to FWP due to the longer absolute traveling length.

Based on the deduced relationships, it can be concluded that when testing the buildability of a material for FP processes, generally higher velocities of the printhead are to be followed during laboratory tests in comparison to corresponding tests for FWP.

5. Conclusions

Buildability – the ability of extruded material to retain its shape and size under sustained loads, has been critically examined in the context of digital construction (DC). Following conclusions can be drawn:

- Fundamental approaches for buildability analyses based on rheological and/or mechanical performance of printable concrete are currently not universally applicable and are to be perceived with priority.
- For wide-range implementation of DC, straightforward and pragmatic test methods without necessity of complex testing equipment (such as rheometers or numerical simulation) are beneficial.
- Claims by several researchers and practitioners with respect to substantial economic savings due to the use of DC are so far not substantiated with comprehensive cost-calculation models.

This paper proposed direct printing tests as a practice-oriented buildability test methodology that is linked to target DC applications. Following are the key aspects to be noted:

- In direct printing tests: what should be the height of the wall to be printed and time intervals applied? These parameters cannot be assumed arbitrarily; a systematic calculation approach based on the targeted applications and in accordance with the developed printing strategy is needed.
- In the proposed approach, the height of the experimental wall was calculated using the aspect ratio of the target construction element.
- The time intervals influence printing time and thus overall costs. In the proposed approach, maximum time interval was determined

considering the minimum printing velocity needed for DC to be economically viable in comparison to conventional construction.
- Since the suggested approach takes machine, labor and material costs into consideration, it can be applied for quantifying the economic viability of DC processes.
- In case of CONPrint3D application for a residential building, a lab-scale wall of 18 layers with a maximum time interval of approximately 52 min was determined as the buildability test specimen. The buildability of a fine-grained, printable concrete was verified for this application scenario.

It was also proven that the buildability test parameters for a given material not only depends upon the target structure, but also on the applied printing process/approach.

- The comparative analyses of full-width printing (FWP) and filament printing (FP) revealed that, assuming the same rate of construction, the buildability of a material for FP processes should be tested, in laboratory experiments, at higher velocities of the printhead than in the case of FWP.
- In addition, a relationship was derived to calculate the printhead velocity needed in the case of FP related to the velocity in FWP, to achieve an equal construction rate.

6. Outlook

Some issues raised in the article at hand are subject of ongoing research. The main ongoing and perspective research activities can be summarized as follows:

- Extension of the cost calculation model to consider additional parameters of digital construction, such as design variations, effective printing velocities due to stops-and-goes at each vertical movement, at the openings, etc.
- A comparative economic viability analysis by applying proposed cost-calculation approach for various digital construction technologies.
- In case of slender elements or high vertical printing rates, buckling plays a significant role. Considering this, the validity of the down-scaled laboratory results for the large-scale construction needs to be reassessed.
- Validation of the approach with full-scale printing tests and with printable concretes containing aggregates with a maximum size of 8 mm.
- Direct buildability tests at various ambient conditions such as temperature, humidity, and wind velocity.

Declaration of Competing Interest

All authors have participated in (a) conception and design, or analysis and interpretation of the data; (b) drafting the article or revising it critically for important intellectual content; and (c) approval of the final version.

This manuscript has not been submitted to, nor is under review at, another journal or other publishing venue.

The following authors have affiliations with organizations with direct or indirect financial interest in the subject matter discussed in the manuscript: Venkatesh Naidu Nerella, Technische Universität Dresden, Institut für Baustoffe; Viktor Mechtcherine, Technische Universität Dresden, Institut für Baustoffe; Martin Krause, Technische Universität Dresden, Institut für Baubetriebswesen.

Acknowledgements

The work presented is a part of the first author's PhD dissertation. Authors express their sincere gratitude to the German Federal Ministry of Interior, Building and Community (BMI) for funding the preceding research projects through the research initiative Zukunft Bau of the Federal Institute for Research on Building, Urban Affairs and Spatial Development (BBSR). Furthermore, the financial support of the German-Czech project digiCON2 - Digital Concrete Construction by the Federal Ministry of Education and Research (BMBF) is highly acknowledged.

References

[1] B. Khoshnevis, Automated construction by contour crafting—related robotics and information technologies, Autom. Constr. 13 (2004) 5–19, https://doi.org/10.1016/j.autcon.2003.08.012.
[2] R.A. Buswell, R.C. Soar, A.G.F. Gibb, A. Thorpe, Freeform construction: mega-scale rapid manufacturing for construction, Autom. Constr. 16 (2007) 224–231, https://doi.org/10.1016/j.autcon.2006.05.002.
[3] E. Dini, D-shape, Monolite-UK-Ltd, https://d-shape.com/, (2015) , Accessed date: 23 August 2015.
[4] TotalKustom, 3D-Printed Hotel, http://www.totalkustom.com/3d-printed-hotel-suite.html, (2015) , Accessed date: 27 April 2016.
[5] C. Gosselin, R. Duballet, P. Roux, N. Gaudillière, J. Dirrenberger, P. Morel, Large-scale 3D printing of ultra-high performance concrete — a new processing route for architects and builders, Mater. Des. 100 (2016) 102–109, https://doi.org/10.1016/j.matdes.2016.03.097.
[6] R.A. Buswell, W.R. Leal de Silva, S.Z. Jones, J. Dirrenberger, 3D printing using concrete extrusion: a roadmap for research, Cem. Concr. Res. 112 (2018) 37–49, https://doi.org/10.1016/j.cemconres.2018.05.006.
[7] E. Lloret, A.R. Shahab, M. Linus, R.J. Flatt, F. Gramazio, M. Kohler, S. Langenberg, Complex concrete structures — merging existing casting techniques with digital fabrication, Comput. Aided Des. 60 (2015) 40–49, https://doi.org/10.1016/j.cad.2014.02.011.
[8] V.N. Nerella, M. Krause, M. Näther, V. Mechtcherine, 3D Printing Technology for On-site Construction, Concrete Plant International, 2016, pp. 36–41 https://www.cpi-worldwide.com/en/journals/artikel/46286 , Accessed date: 25 September 2019.
[9] G. Cesaretti, E. Dini, X. De Kestelier, V. Colla, L. Pambaguian, Building components for an outpost on the Lunar soil by means of a novel 3D printing technology, Acta Astronautica 93 (2014) 430–450, https://doi.org/10.1016/j.actaastro.2013.07.034.
[10] D. Lowke, E. Dini, A. Perrot, D. Weger, C. Gehlen, B. Dillenburger, Particle-bed 3D printing in concrete construction — possibilities and challenges, Cem. Concr. Res. 112 (2018) 50–65, https://doi.org/10.1016/j.cemconres.2018.05.018.
[11] Apis-cor, Apis Cor — construction technology, http://apis-cor.com/en/faq/texnologiya-stroitelstva/, (2017) , Accessed date: 29 December 2017.
[12] A. Pierre, D. Weger, A. Perrot, D. Lowke, Penetration of cement pastes into sand packings during 3D printing: analytical and experimental study, Mater. Struct. 51 (2018) 22, https://doi.org/10.1617/s11527-018-1148-5.
[13] R.A. Buswell, a Thorpe, R.C. Soar, A.G.F. Gibb, Design, data and process issues for mega-scale rapid manufacturing machines used for construction, Autom. Constr. 17 (2008) 923–929, https://doi.org/10.1016/j.autcon.2008.03.001.
[14] T.T. Le, S.A. Austin, S. Lim, R.A. Buswell, A.G.F. Gibb, T. Thorpe, Mix design and fresh properties for high-performance printing concrete, Mater. Struct. 45 (2012) 1221–1232, https://doi.org/10.1617/s11527-012-9828-z.
[15] V. Mechtcherine, V.N. Nerella, K. Kasten, Testing pumpability of concrete using sliding pipe rheometer, Constr. Build. Mater. 53 (2014) 312–323, https://doi.org/10.1016/j.conbuildmat.2013.11.037.
[16] D. Feys, K.H. Khayat, R. Khatib, How do concrete rheology, tribology, flow rate and pipe radius influence pumping pressure? Cem. Concr. Compos. 66 (2016) 38–46, https://doi.org/10.1016/j.cemconcomp.2015.11.002.
[17] V.N. Nerella, M. Näther, A. Iqbal, M. Butler, V. Mechtcherine, Inline quantification of extrudability of cementitious materials for digital construction, Cem. Concr. Compos. 95 (2019) 260–270, https://doi.org/10.1016/j.cemconcomp.2018.09.015.
[18] S. Lim, R.A. Buswell, T.T. Le, S.A. Austin, A.G.F. Gibb, T. Thorpe, Developments in construction-scale additive manufacturing processes, Autom. Constr. 21 (2012) 262–268, https://doi.org/10.1016/j.autcon.2011.06.010.
[19] A. Kazemian, X. Yuan, E. Cochran, B. Khoshnevis, Cementitious materials for construction-scale 3D printing: laboratory testing of fresh printing mixture, Constr. Build. Mater. 145 (2017) 639–647, https://doi.org/10.1016/j.conbuildmat.2017.04.015.
[20] T. Wangler, E. Lloret, L. Reiter, N. Hack, F. Gramazio, M. Kohler, M. Bernhard, B. Dillenburger, J. Buchli, N. Roussel, R. Flatt, Digital concrete: opportunities and challenges, RILEM Technical Letters 1 (2016) 67–75, https://doi.org/10.21809/rilemtechlett.2016.16.
[21] D. Marchon, S. Kawashima, H. Bessaies-Bey, S. Mantellato, S. Ng, Hydration and rheology control of concrete for digital fabrication: potential admixtures and cement chemistry, Cem. Concr. Res. 112 (2018) 96–110, https://doi.org/10.1016/j.cemconres.2018.05.014.
[22] L. Reiter, T. Wangler, N. Roussel, R.J. Flatt, The role of early age structural build-up in digital fabrication with concrete, Cem. Concr. Res. 112 (2018) 86–95, https://doi.org/10.1016/j.cemconres.2018.05.011.
[23] WinSun Kira, China builds world's first 3D printed villa and tallest 3D printed apartment building, 3ders, http://www.3ders.org/articles/20150118-winsun-

builds-world-first-3d-printed-villa-and-tallest-3d-printed-building-in-china.html, (2015) , Accessed date: 25 January 2016.
[24] F. Bos, R. Wolfs, Z. Ahmed, T. Salet, Additive manufacturing of concrete in construction: potentials and challenges of 3D concrete printing, Virtual and Physical Prototyping 11 (2016) 209–225, https://doi.org/10.1080/17452759.2016.1209867.
[25] B. García de Soto, I. Agustí-Juan, J. Hunhevicz, S. Joss, K. Graser, G. Habert, B.T. Adey, Productivity of digital fabrication in construction: cost and time analysis of a robotically built wall, Autom. Constr. 92 (2018) 297–311, https://doi.org/10.1016/j.autcon.2018.04.004.
[26] G. De Schutter, K. Lesage, V. Mechtcherine, V.N. Nerella, G. Habert, I. Agusti-Juan, Vision of 3D printing with concrete — technical, economic and environmental potentials, Cem. Concr. Res. 112 (2018) 25–36, https://doi.org/10.1016/j.cemconres.2018.06.001.
[27] P. Wu, J. Wang, X. Wang, A critical review of the use of 3-D printing in the construction industry, Autom. Constr. 68 (2016) 21–31, https://doi.org/10.1016/j.autcon.2016.04.005.
[28] J. Zhang, B. Khoshnevis, Optimal machine operation planning for construction by contour crafting, Autom. Constr. 29 (2013) 50–67, https://doi.org/10.1016/j.autcon.2012.08.006.
[29] S. Lim, R.A. Buswell, P.J. Valentine, D. Piker, S.A. Austin, X. De Kestelier, Modelling curved-layered printing paths for fabricating large-scale construction components, Additive Manufacturing (2016), https://doi.org/10.1016/j.addma.2016.06.004.
[30] N. Labonnote, A. Rønnquist, B. Manum, P. Rüther, A. R??nnquist, B. Manum, P. R??ther, Additive construction: state-of-the-art, challenges and opportunities, Autom. Constr. 72 (2016) 347–366, https://doi.org/10.1016/j.autcon.2016.08.026.
[31] G.W. Ma, L. Wang, Y. Ju, State-of-the-art of 3D printing technology of cementitious material—an emerging technique for construction, SCIENCE CHINA Technol. Sci. 149 (2017) 1–21, https://doi.org/10.1007/s11431-016-9077-7.
[32] T. Di Carlo, A. Carlson, B. Khoshnevis, T. Di Carlo, Experimental and Numerical Techniques to characterize Structural Properties of Fresh concrete, University of Southern California (2013), http://digitallibrary.usc.edu/cdm/ref/collection/p15799coll3/id/107132 , Accessed date: 29 September 2018.
[33] B. Panda, S.C. Paul, N.A.N. Mohamed, Y.W.D. Tay, M.J. Tan, Measurement of tensile bond strength of 3D printed geopolymer mortar, Measurement 113 (2018) 108–116, https://doi.org/10.1016/j.measurement.2017.08.051.
[34] N. Roussel, Rheological requirements for printable concretes, Cem. Concr. Res. 1–10 (2018), https://doi.org/10.1016/j.cemconres.2018.04.005.
[35] A. Perrot, D. Rangeard, A. Pierre, Structural built-up of cement-based materials used for 3D-printing extrusion techniques, Mater. Struct. 49 (2016) 1213–1220, https://doi.org/10.1617/s11527-015-0571-0.
[36] N. Roussel, A thixotropy model for fresh fluid concretes: theory, validation and applications, Cem. Concr. Res. 36 (2006) 1797–1806, https://doi.org/10.1016/j.cemconres.2006.05.025.
[37] A. Perrot, A. Pierre, S. Vitaloni, V. Picandet, Prediction of lateral form pressure exerted by concrete at low casting rates, Mater. Struct. 48 (2015) 2315–2322, https://doi.org/10.1617/s11527-014-0313-8.
[38] Y. Weng, M. Li, M.J. Tan, S. Qian, Design 3D printing cementitious materials via fuller Thompson theory and Marson-Percy model, Constr. Build. Mater. 163 (2018) 600–610, https://doi.org/10.1016/j.conbuildmat.2017.12.112.
[39] N. Roussel, C. Lanos, Plastic fluid flow parameters identification using a simple squeezing test, Appl. Rheol. 13 (2003) 132–141, https://doi.org/10.3933/ApplRheol-13-132.
[40] R.J.M. Wolfs, F.P. Bos, T.A.M. Salet, Early age mechanical behaviour of 3D printed concrete: numerical modelling and experimental testing, Cem. Concr. Res. 106 (2018) 103–116, https://doi.org/10.1016/j.cemconres.2018.02.001.
[41] D. Feys, G. De Schutter, K.H. Khayat, R. Verhoeven, Changes in rheology of self-consolidating concrete induced by pumping, Mater. Struct. 49 (2016) 4657–4677, https://doi.org/10.1617/s11527-016-0815-7.
[42] T.T. Le, S.A. Austin, S. Lim, R.A. Buswell, R. Law, A.G.F. Gibb, T. Thorpe, Hardened properties of high-performance printing concrete, Cem. Concr. Res. 42 (2012) 558–566, https://doi.org/10.1016/j.cemconres.2011.12.003.
[43] B. Panda, S.C. Paul, M.J. Tan, Anisotropic mechanical performance of 3D printed fiber reinforced sustainable construction material, Mater. Lett. (2017), https://doi.org/10.1016/j.matlet.2017.07.123.
[44] Y.W.D. Tay, G.H.A. Ting, Y. Qian, B. Panda, L. He, M.J. Tan, Time gap effect on bond strength of 3D-printed concrete, Virtual and Physical Prototyping 14 (2019) 104–113, https://doi.org/10.1080/17452759.2018.1500420.
[45] Totalkustom, 3D printed castle — photo gallery, http://www.totalkustom.com/photo.html, (2015) , Accessed date: 29 December 2017.
[46] V. Mechtcherine, V.N. Nerella, F. Will, M. Näther, J. Otto, M. Krause, Large-scale digital concrete construction — CONPrint3D concept for on-site, monolithic 3D-printing, Autom. Constr. 107 (2019) 102933, , https://doi.org/10.1016/J.AUTCON.2019.102933.
[47] A.S.J. Suiker, Mechanical performance of wall structures in 3D printing processes: theory, design tools and experiments, Int. J. Mech. Sci. 137 (2018) 145–170, https://doi.org/10.1016/j.ijmecsci.2018.01.010.
[48] F. Mahaut, S. Mokéddem, X. Chateau, N. Roussel, G. Ovarlez, Effect of coarse particle volume fraction on the yield stress and thixotropy of cementitious materials, Cem. Concr. Res. 38 (2008) 1276–1285, https://doi.org/10.1016/j.cemconres.2008.06.001.
[49] Deutsches-Institut-für-Normung-e.-V, DIN 18202:2013-04 — Tolerances in Building Construction — Buildings, Beuth Verlag, Germany, 2013. https://www.beuth.de/en/standard/din-18202/170362951 (accessed February 7, 2017). doi:10.31030/1939749.
[50] BKI Baukosteninformationszentrum – Baukosten Gebäude Neubau 2017 — Statistische Kostenkennwerte (English translation: Construction costs of buildings, for new buildings 2017 - statistical cost parameters), Baukosteninformationszentrum Deutscher Architektenkammern GmbH, Stuttgart, 2017. ISBN: 9783481036331.
[51] Hauptverband der Deutschen Bauindustrie, BGL Baugeräteliste 2015 — Technisch-wirtschaftliche Baumaschinendaten (English translation: BGL construction machine list 2015 - Technical and economic data of construction machinery), Bauverlag BV GmbH, Gütersloh, 2015. ISBN: 9783762536703.
[52] Y. Chen, F. Veer, O. Çopuroğlu, A critical review of 3D concrete printing as a low CO2 concrete approach, HERON 62 (2017) 167–194, https://doi.org/10.13140/RG.2.2.12323.71205.
[53] V.N. Nerella, S. Hempel, V. Mechtcherine, Micro- and macroscopic investigations on the interface between layers of 3d-printed cementitious elements, in: M. Santhanam, R. Gettu, R.G. Pillai, S.K. Nayar (Eds.), International Conference on Advances in Construction Materials and Systems (ICACMS), 3 RILEM Publications SARL, Chennai, 978-2-35158-190-2, 2017, pp. 557–565.
[54] C. Schröfl, V.N. Nerella, V. Mechtcherine, Capillary water intake by 3D-printed concrete visualised and quantified by neutron radiography, in: T. Wangler, R.J. Flatt (Eds.), First RILEM International Conference on Concrete and Digital Fabrication - Digital Concrete 2018, Springer International Publishing, Zürich, 2019, pp. 217–224, , https://doi.org/10.1007/978-3-319-99519-9.
[55] Cooper Hewitt, Why Design Now?: Contour Crafting - YouTube, https://www.youtube.com/watch?v=-yv-IWdSdns, (2010) , Accessed date: 14 March 2016.
[56] D. Hwang, B. Khoshnevis, Concrete wall fabrication by contour crafting, ISARC 2004 21st International Symposium on Automation and Robotics in Construction, The International Association for Automation and Robotics in Construction, 2004.